

Robust fuzzy local information and L_p -norm distance-based image segmentation method

ISSN 1751-9659

Received on 9th July 2016

Revised 23rd November 2016

Accepted on 28th December 2016

E-First on 25th January 2017

doi: 10.1049/iet-ipr.2016.0539

www.ietdl.org

Fang Li¹ ✉, Jing Qin²¹Department of Mathematics, East China Normal University, Shanghai, People's Republic of China²Department of Mathematical Sciences, Montana State University, Bozeman, MT, USA

✉ E-mail: fli@math.ecnu.edu.cn

Abstract: A variant of fuzzy c-means (FCM) clustering algorithm for image segmentation is provided. Unlike the L_2 -norm distance in FCM, L_p with $p \in (0, 1]$ norm is used to measure the distance of the pixel intensity to its cluster centre in the energy functional. Moreover, local spatial information and colour information are incorporated into the model to enhance the robustness to noise and outliers. The proposed algorithm is called fuzzy local information L_p (FLILp) clustering. To overcome the difficulty of finding cluster centres, L_p -norm distance is approximated by weighted L_2 distance. The advantages of FLILp are: (i) it is strongly robust to noise and outliers, (ii) it is applied to the original image and (iii) it preserves image edges. Numerical examples and comparisons of image segmentation on both synthetic and real images illustrate the outstanding performance and robustness of the proposed method.

1 Introduction

Image segmentation is one of the most important topics in image processing and computer vision. It aims to partition an image into non-overlapped, consistent regions which are homogeneous with respect to some characteristics such as intensity, colour or texture. Various methods have been proposed in the literature for image segmentation which can be mainly classified into five categories: thresholding, clustering, edge detection, region extraction and saliency detection, see [1–9] and references therein. In this paper, we focus on clustering methods for image segmentation.

There are two major types of clustering methods: hard clustering methods and fuzzy clustering methods [10–15]. In hard clustering, each point of the data set belongs exclusively to one cluster. By contrast, in fuzzy clustering, each point can be simultaneously in several classes with some probability which is represented by a fuzzy membership function. In many real applications such as medical imaging and remote sensing imaging, the acquired images usually have limited spatial resolution and low contrast such that hard clustering may fail to identify clusters. Hence, fuzzy clustering is more appropriate than hard clustering for solving image segmentation problems.

One of the most popular fuzzy clustering methods is the fuzzy c-means (FCM) clustering algorithm, which was introduced by Dunn [11] and then developed by Bezdek [10, 16]. FCM is widely used in data mining and image segmentation. The advantages of FCM include a straightforward implementation, fairly robust behaviour, applicability in multichannel data and the ability to model uncertainty within the data [17]. FCM works well on most noise-free images. However, a major disadvantage of FCM when used in image segmentation is its extreme sensitivity to noise and other imaging artefacts. The reason is that the clustering process of FCM is totally decided by image intensity/colour information without considering the spatial connection of pixels.

One natural approach to enhance the robustness of FCM in image segmentation is to smooth the image before applying FCM. However, it is very difficult to control the trade-off between smoothing and clustering. Thus, many other approaches consider to incorporate local spatial information into FCM to enhance the segmentation accuracy (SA) [17–31]. In this paper, we focus on the FCM variants which have the simple solution framework as FCM. That is, the membership functions can be solved directly from the

energy minimisation problem in a similar way as FCM. In what follows, we will briefly review those methods.

Pham [17, 28] generalised the FCM objective function to include a spatial penalty term on the membership functions to enforce the spatial smoothness, which is called the robust fuzzy C-means algorithm.

Ahmed *et al.* [18] proposed FCM_S by modifying the objective function of the standard FCM to compensate the intensity inhomogeneity and allow the labelling of a pixel to be influenced by the labels in its immediate neighbourhood.

To reduce the computational complexity of FCM_S, Chen and Zhang [21] proposed two variants, FCM_S1 and FCM_S2, which simplifies the neighbourhood term of the objective function of FCM_S by introducing the extra mean-filtered image and median-filtered image to replace the neighbourhood term of FCM_S.

Szilágyi *et al.* [30] proposed the enhanced fuzzy c-mean (EnFCM) algorithm to accelerate the image segmentation process. Firstly, a linearly weighted sum image is formed in advance from both original image and its local neighbour average grey image. Then EnFCM performs clustering on the grey-level histogram instead of pixels in the summed image. Since the number of grey levels is much smaller than the number of pixels, EnFCM is much faster than FCM_S. Besides, the quality of image segmented by EnFCM is comparable to that of FCM_S.

Cai *et al.* [20] proposed the fast generalised fuzzy c-means (FGFCM) algorithm for fast and robust image segmentation. FGFCM incorporates local spatial and grey information to form a new image in advance. The clustering process is then performed on the histogram of the new image. Furthermore, Cai *et al.* also proposed two variants of FGFCM, FGFCM_S1 and FGFCM_S2, by modifying the local similarity measure as mean and median.

More recently, Krinidis and Chatzis [24] proposed a robust fuzzy local information c-means clustering algorithm (FLICM). Specifically, the key ingredient of FLICM is the use of a fuzzy local (both spatial and grey level) similarity measure, which is aimed at guaranteeing noise insensitiveness and image detail preservation. Thus FLICM has advantages such as noise immunity and free of artificial parameters. However, the noise immunity of FLICM is still limited, especially for high levels of noise.

In the aforementioned algorithms, L_2 -norm-based distance is used in the objective functions. By contrast, L_p -norm ($0 < p \leq 1$)-based distance is rarely studied in fuzzy clustering algorithms [32–

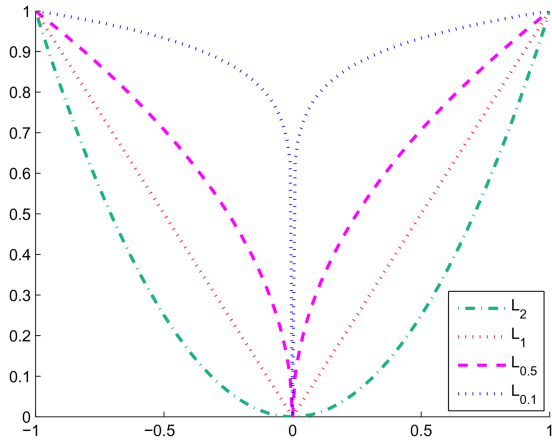


Fig. 1 L_p functions with $p = 2, 1, 0.5, 0.1$, respectively

35]. In particular, the subproblem involving cluster centres is in general difficult to solve. One of the most common methods is bisection searching method point by point which is time consuming. However, L_p -norm ($p = 1$)-based fidelity has shown to be more robust to impulse noise, outliers and other artefacts than its L_2 counterpart especially in image restoration problems [36, 37]. The basic reason is that L_p -norm ($p \leq 1$) induces higher sparsity than L_2 -norm such that the former is able to provide a better statistical description of noise and artefacts in images. In Fig. 1, we display the functions of L_p with $p = 2, 1, 0.5, 0.1$, respectively. It is obvious that L_p with $p = 1, 0.5, 0.1$ have higher sparsity than L_2 . So far as we know, the local information has not been considered in the existing L_p -norm ($p \neq 2$)-based fuzzy clustering algorithms. These are the motivations of us to consider L_p -norm distance and incorporate local information into the fuzzy clustering process.

In this paper, we propose a fuzzy clustering algorithm based on local spatial/colour information of an image and L_p -norm distance, abbreviated as FLILp, to further enhance segmentation performance and robustness. Based on some approximation of the energy function, the corresponding numerical algorithm can be derived in a similar way as FCM. Namely, subproblems involving the membership functions and class centres have closed-form solutions. Experiments on synthetic grey images and real colour images demonstrate the effectiveness of the proposed algorithm.

This paper is organised as follows: In Section 2, we review the FCM clustering algorithm and its variants with spatial constraint, including FCM_S1, FCM_S2, EnFCM, FGFCM, FGFCM_S1, FGFCM_S2 and FLICM. Then we propose the new algorithm FLILp in Section 3. The numerical experiments are displayed in Section 4. The conclusion is given at Section 5.

2 Related methods

2.1 FCM

The objective function in a standard FCM [10] for partitioning a dataset $\{x_i\}_{i=1}^N$ into c clusters is given by

$$J_m = \sum_{k=1}^c \sum_{i=1}^N u_{ki}^m \|x_i - v_k\|^2 \quad (1)$$

where $\|\cdot\|$ denotes the Euclidean distance, $\{v_k\}_{k=1}^c$ is the centres of the clusters and the array $[u_{ki}] = U$ represents a partition matrix (or membership functions), $U \in \mathcal{U}$, that is

$$\mathcal{U} = \left\{ u_{ki} \in [0, 1] \left| \sum_{k=1}^c u_{ki} = 1 \quad \forall i \quad \text{and} \quad \sum_{i=1}^N u_{ki} > 0 \quad \forall k \right. \right\}. \quad (2)$$

The parameter m is a weighting exponent on each membership function which determines the fuzziness of the resulting classification.

2.2 FCM_S, FCM_S1 and FCM_S2

FCM_S [18] is a modification of FCM by introducing a term that allows the labelling of a pixel to be influenced by the labels in its immediate neighbourhood. The neighbourhood effect acts as a regulariser which enforces the piecewise homogeneity of the solution. Such regularisation is useful in segmenting scans corrupted by noise. The modified objective function of FCM_S is as follows:

$$J_m = \sum_{k=1}^c \sum_{i=1}^N u_{ki}^m \|x_i - v_k\|^2 + \frac{\alpha}{N_R} \sum_{k=1}^c \sum_{i=1}^N u_{ki}^m \left(\sum_{r \in \mathcal{N}_i} \|x_r - v_k\|^2 \right) \quad (3)$$

where x_i is the grey-level value of the i th pixel, N is the total number of pixels, v_k represents the prototype value of the k th cluster, u_{ki} represents the fuzzy membership of the i th pixel with respect to cluster k , x_r represents the neighbour of x_i , \mathcal{N}_i stands for the set of neighbours that exists in a window around x_i and N_R is the cardinality of \mathcal{N}_i . The effect of neighbours term is controlled by the weighted parameter α .

FCM_S1 and FCM_S2 [21] are variants of FCM_S, where the neighbourhood term is simplified. The objective function is given by

$$J_m = \sum_{k=1}^c \sum_{i=1}^N u_{ki}^m \|x_i - v_k\|^2 + \alpha \sum_{k=1}^c \sum_{r \in \mathcal{N}_i} u_{ki}^m \|\bar{x}_r - v_k\|^2 \quad (4)$$

where \bar{x}_r is the average (FCM_S1) or median (FCM_S2) of neighbouring pixels lying within a window around x_r . \bar{x}_r can be computed in advance as mean-filtered image and median-filtered image, respectively. Therefore the whole computational time is reduced compared with FCM_S.

2.3 EnFCM

EnFCM [30] is proposed to accelerate FCM_S. Firstly, a new image ξ is calculated in advance

$$\xi_i = \frac{1}{1 + \alpha} \left(x_i + \frac{\alpha}{N_R} \sum_{j \in \mathcal{N}_i} x_j \right).$$

Then the clustering is performed on the grey-level histogram of the image ξ . The objective function of EnFCM is defined as

$$J_m = \sum_{k=1}^c \sum_{l=1}^M \gamma_l u_{kl}^m (\xi_l - v_k)^2$$

where M denotes the number of grey levels of image ξ , and γ_l is the number of pixels having grey-level value equal to l . In other words, EnFCM performs FCM in the 1D range of the image ξ . Since the number of grey-levels M ($M = 256$ for 8 bit grey-level image) are generally much smaller than the total number of pixels N , EnFCM is computationally very efficient.

2.4 FGFCM, FGFCM_S1 and FGFCM_S2

FGFCM [20] is proposed to improve the clustering result and facilitate the choice of parameter. A local similarity measure is introduced in FGFCM as follows:

$$S_{ij} = \begin{cases} 0, & i = j \\ \exp\left(-\frac{\max(|p_i - p_j|, |q_i - q_j|)}{\lambda_s} - \frac{\|x_i - x_j\|^2}{\lambda_g \sigma_i^2}\right), & i \neq j \end{cases}$$

where (p_i, q_i) is the coordinates of pixel i , λ_s and λ_g are two scale factors playing a role similar to α in the aforementioned methods, and σ_i is defined as

$$\sigma_i = \sqrt{\frac{\sum_{j \in \mathcal{N}_i} \|x_i - x_j\|^2}{N_R}}$$

Note that S_{ij} measures the similarity between the i th pixel and the j th pixel. Then a linearly weighted summed image is generated as

$$\xi_i = \frac{\sum_{j \in \mathcal{N}_i} S_{ij} x_j}{\sum_{j \in \mathcal{N}_i} S_{ij}}$$

In the final step of FGFCM, FCM is applied on the range of ξ .

FGFCM_S1 and FGFCM_S2 are variants of FGFCM which incorporate modified similarity measures in their respective objective functions. In other words, FGFCM_S1 and FGFCM_S2 regard mean-filtered image and median-filtered image as the new image ξ , respectively.

2.5 FLICM

FLICM [24] is characterised by the use of a fuzzy local similarity measure, which aims at guaranteeing noise insensitiveness and image detail preservation. In particular, a novel fuzzy factor is introduced into the objective function of FLICM to enhance the clustering performance. This fuzzy factor is defined as

$$G_{ki} = \sum_{j \in \mathcal{N}_i, i \neq j} \frac{1}{d_{ij} + 1} (1 - u_{kj})^m \|x_j - v_k\|^2$$

where d_{ij} is the spatial Euclidean distance of the i th pixel and j th pixel. The objective function of FLICM is given by

$$J_m = \sum_{i=1}^c \sum_{k=1}^N (u_{ki}^m \|x_k - v_i\|^2 + G_{ki}).$$

FLICM performs quite well on images with low levels of noise.

3 Proposed FLILp method

In this section, we propose a novel fuzzy local information and L_p -norm distance-based clustering method for image segmentation, which is called FLILp.

3.1 FLILp objective function

To enhance the segmentation performance and robustness, we propose a new algorithm which combines the advantages of FLICM algorithm and the robustness of L_p -norm distance. More specifically, in the objective function, we incorporate the local information and use L_p -norm to measure the distance between pixel values and class centres.

Firstly, we consider the case of grey-level images, i.e. $x_i \in \mathbb{R}$. Let $p \in (0, 1]$. We denote the local window centred at x_i by \mathcal{N}_i . Let u_{kj} be the degree of membership of the j th pixel in the k th cluster with centre v_k . We also construct a symmetric matrix \mathbf{K} whose (i, j) th entry measures the spatial similarity of the i th pixel and the j th pixel. The objective function of the proposed FLILp method is as follows:

$$J_m = \sum_{i=1}^N \sum_{k=1}^c u_{ki}^m (\|x_i - v_k\|^p + \alpha G_{ki}). \quad (5)$$

where $\|\cdot\|$ denotes the Euclidean distance. Here G_{ki} is the L_p -norm-based local factor introduced to incorporate the local information, which is defined as

$$G_{ki} = \sum_{j \in \mathcal{N}_i} K_{ij} (1 - u_{kj})^m \|x_j - v_k\|^p. \quad (6)$$

In (5), $\alpha > 0$ is a weighting parameter to control the contribution of the local factor. Note that α is fixed as 1 in FLICM. Here we introduce this parameter since it contributes to noise robustness in our method. As the noise-level increases, we choose large values for α to achieve the best performance.

Similar to FLICM, one choice of K_{ij} is

$$K_{ij} = \begin{cases} 0, & i = j \\ \frac{1}{d_{ij} + 1}, & i \neq j \end{cases} \quad (7)$$

where d_{ij} is the spatial Euclidean distance of the i th pixel and j th pixel. Another choice is setting $K_{ij} = 1$ in the above formula and then normalising the kernel to satisfy the sum-to-one constraint. Other choices of K_{ij} include Gaussian kernel and mean kernel.

Let us give an interpretation of local factor G_{ki} . For each pixel i , assume $u_{ki} \simeq 1$, that is, x_i has a large probability of belonging to the k th class. Assume pixel j has similar spatial location and grey value as pixel i , namely $j \in \mathcal{N}_i$ and $x_i \simeq x_j$. Thus $\|x_j - v_k\|^p \simeq \|x_i - v_k\|^p$. To minimise the energy function (5), $(1 - u_{kj})^m$ is forced to approach zero, such that $u_{kj} \simeq 1$. Hence, we conclude that $u_{ki} \simeq u_{kj}$ if $j \in \mathcal{N}_i$ and $x_i \simeq x_j$. That is, if two pixels have similar grey-level values and similar spatial location, they tend to be in the same cluster by minimising the objective function. Moreover, by using the spatial kernel K_{ij} , the local factor G_{ki} has more flexibility to adjust the influence of neighbouring pixels. In conclusion, the effect of the local factor G_{ki} to allows the labelling of a pixel to be influenced by its immediate neighbourhood both in spatial domain and range.

3.2 FLILp algorithm

Similar to FCM, we apply the alternating minimisation method to derive an efficient algorithm to solve the FLILp model (5).

3.2.1 Membership functions estimation: Let us simplify the proposed objective function in (5) as

$$J_m = \sum_{k=1}^c \sum_{i=1}^N u_{ki}^m D_{ki} \quad (8)$$

where

$$D_{ki} = \|x_i - v_k\|^p + \alpha G_{ki}.$$

Since $[u_{ki}] \in \mathcal{U}$ satisfies the sum-to-one constraint and the non-negativity constraint in (2), we introduce N Lagrange multipliers $\lambda_i, i = 1, \dots, N$ and then minimise

$$F_m = \sum_{k=1}^c \sum_{i=1}^N u_{ki}^m D_{ki} + \sum_{i=1}^N \lambda_i \left(1 - \sum_{k=1}^c u_{ki}\right). \quad (9)$$

By taking the derivative of F_m with respect to u_{ki} and setting the result to zero, we have, for $m > 1$

$$\frac{\partial F_m}{\partial u_{ki}} = m u_{ki}^{m-1} D_{ki} - \lambda_i = 0. \quad (10)$$

Then we have

$$u_{ki} = \left(\frac{\lambda_i}{mD_{ki}} \right)^{1/(m-1)}. \quad (11)$$

Using the condition $\sum_{k=1}^c u_{ki} = 1 \quad \forall i$, we get

$$\lambda_i = \frac{m}{\left(\sum_{k=1}^c (1/D_{ki})^{1/(m-1)} \right)^{m-1}}. \quad (12)$$

Substituting (12) into (11), we get the updating formula of membership functions as

$$u_{ki} = \frac{1}{\sum_{j=1}^c (D_{ki}/D_{kj})^{1/(m-1)}}. \quad (13)$$

3.2.2 Cluster centres estimation: The second term of the proposed objective function (5) can be reformulated as

$$\begin{aligned} & \sum_{k=1}^c \sum_{i=1}^N \sum_{j \in N_i} u_{ki}^m K_{ij} (1 - u_{kj})^m \|x_j - v_k\|^p \\ &= \sum_{k=1}^c \sum_{j=1}^N \sum_{i \in N_j} u_{ki}^m K_{ji} (1 - u_{ki})^m \|x_i - v_k\|^p \\ &= \sum_{k=1}^c \sum_{i=1}^N \left(\sum_{j \in N_i} u_{kj} K_{ij} \right) (1 - u_{ki})^m \|x_i - v_k\|^p \\ &= \sum_{k=1}^c \sum_{i=1}^N (\mathbf{K} * u_{ki}^m) (1 - u_{ki})^m \|x_i - v_k\|^p \end{aligned}$$

where $*$ represents the discrete convolution operator. Note that the second equality is obtained by exchanging the indices i and j of the first expression, and the last equality follows from the symmetry property of the kernel \mathbf{K} . Then we can rewrite the objective function (5) as

$$J_m = \sum_{k=1}^c \sum_{i=1}^N (u_{ki}^m + \alpha (\mathbf{K} * u_{ki}^m) (1 - u_{ki})^m) \|x_k - v_i\|^p. \quad (14)$$

To solve v_i , we treat the above L_p -norm as weighted L_2 -norm, namely

$$J_m = \sum_{k=1}^c \sum_{i=1}^N w_{ki} \|x_k - v_i\|^2 \quad (15)$$

where the weight is defined as

$$w_{ki} = \frac{u_{ki}^m + \alpha (\mathbf{K} * u_{ki}^m) (1 - u_{ki})^m}{\|x_i - v_k^e\|^{2-p}}, \quad (16)$$

and v_k^e denotes the estimated value of the centres of clusters. In this paper, we set v_k^e as the class centres in the last iteration. Then we obtain the solution of v_k as

$$v_k = \frac{\sum_{i=1}^N w_{ki} x_i}{\sum_{i=1}^N w_{ki}}. \quad (17)$$

Thus, the proposed FLILp clustering algorithm can be summarised in Algorithm 1.

Algorithm 1: FLILp

1) Set the number of clusters c , fuzziness parameter m and the tolerance ϵ .

2) Initialise cluster centres $\{v_k\}_{k=1}^c$ and fuzzy membership functions $\{u_{ki}\} \in \mathcal{U}$.

3) Update the membership functions using (13).

4) Update the centres of clusters using (17).

Repeat steps 3 and 4 until the stopping criterion is satisfied. The stopping criterion is set as

$$\|V_{\text{new}} - V_{\text{old}}\| \leq \epsilon$$

where $V = (v_1, v_2, \dots, v_c)$ is the vector of cluster centres.

The final crisp segmentation result is obtained by the maximum membership procedure. This procedure assigns the pixel i to the class C with the maximum membership

$$C_i = \arg \{ \max_k \{u_{ki}\} \}, \quad k = 1, 2, \dots, c.$$

3.3 Generalisation to vector-valued image

The proposed algorithm can be easily generalised to vector-valued images. Assume $\mathbf{x}_j = (x_{j1}, \dots, x_{jd}) \in \mathbb{R}^d$ and $\mathbf{v}_k = (v_{k1}, \dots, v_{kd}) \in \mathbb{R}^d$. Then we define the L_p -norm distance term for vector-valued data in the objective function (5) as

$$\|\mathbf{x}_j - \mathbf{v}_k\|^p = \left(\sqrt[p]{\sum_{d=1}^s |x_{jd} - v_{kd}|^2} \right)^p. \quad (18)$$

Similar to the grey-level image case, we can derive the updating formulas for membership functions and centres. We omitted the details for simplicity.

It is worth noting that the L_p -norm distance term defined in (18) is essentially a joint $L_2 - L_p$ norm, which considers the relation of different channels of the image. The special case of (18) when $p = 1$ is also different from the existing L_1 -norm distance [32]

$$\|\mathbf{x}_j - \mathbf{v}_k\|_1 = \sum_{d=1}^s |x_{jd} - v_{kd}| \quad (19)$$

where the channels are separated.

4 Experimental results

In this section, we show the performance of the proposed method FLILp by presenting experimental results on various synthetic and real images, with different levels of Gaussian noise (GN) and salt and pepper noise (SPN). Moreover, we compare the proposed algorithm with eight closely related fuzzy clustering algorithms, including FCM, FCM_S1, FCM_S2, EnFCM, FGFCM, FGFCM_S1, FGFCM_S2 and FLICM. For quantitative analysis of segmentation results, we use SA as performance measure which is defined as [18]

$$SA = \frac{\text{\#correctly classified pixels}}{\text{\#all pixels}}.$$

The number of correctly classified pixels is calculated as follows. Constructing two index images correspond to the crisp segmentation result (denoted as I_1) and the ground truth segmentation (denoted as I_2) by integers $1, 2, \dots, c$ according to the ascending order of pixel's mean value of each class. Then the number of correctly classified pixels is obtained by counting the number of pixels x which satisfy $I_1(x) = I_2(x)$.

In our experiments, for all the methods, we set $m = 2$, $\epsilon = 1e^{-5}$ and maximum iteration number as 500. The window size is set as 3×3 or 5×5 , the weighting parameter α is set as an integer varying from 1 to 20 for all methods involving this parameter. Then we choose the result of each method with best performance. The kernel (7) is used in both FLICM and the proposed FLILp

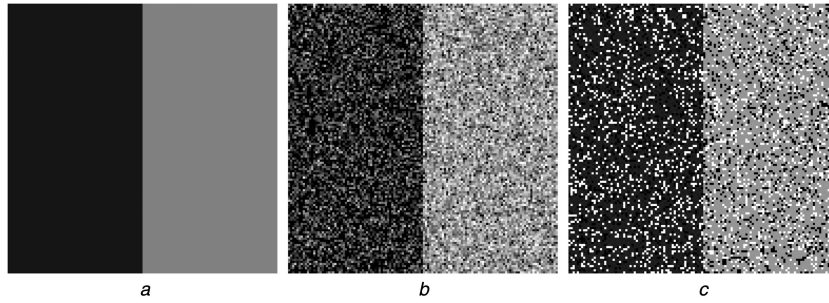


Fig. 2 Two-phase synthetic image and noisy images

(a) Original: The clean synthetic image with grey-level values 20 and 128, (b) Noisy: The noisy image corrupted by GN with mean zero and standard deviation $\sigma = 60$, (c) Noisy: The noisy image corrupted by 30% SPN

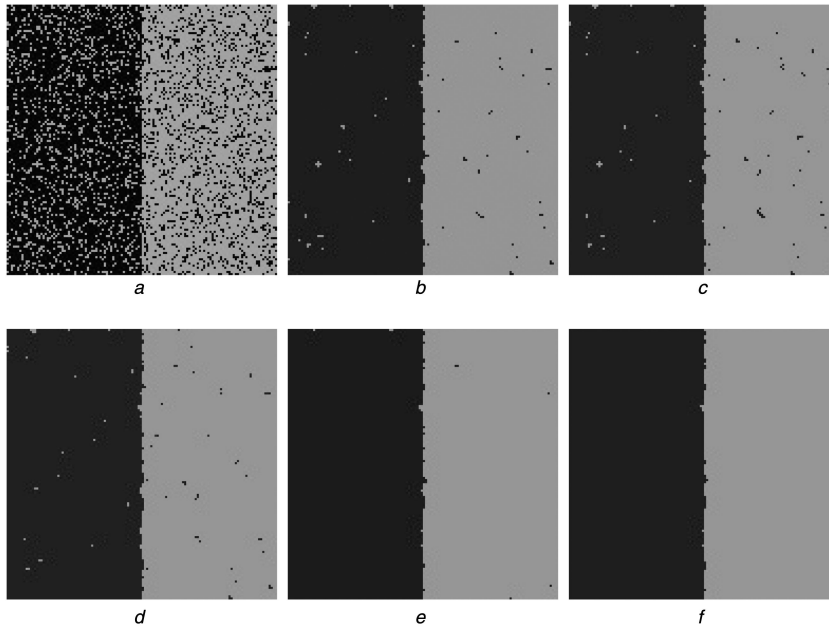


Fig. 3 Two-phase segmentation of a synthetic image corrupted by GN

(a) FCM result, 0.8161; (b) FCM_S1 result, 0.9919; (c) EnFCM result, 0.9915; (d) FGFCM_S1 result, 0.9927; (e) FLICM result, 0.9974; (f) FLILp result, 0.9979. The SA values are reported below each segmentation result

algorithms. In FGFCM, we set $\lambda_s = \lambda_g = 3$. For two-phase segmentation, the membership functions are set as $u_{1i} = \tilde{x}_i$ where \tilde{x}_i is the normalised image into $[0, 1]$ and $u_{2i} = 1 - u_{1i}$. For multiphase segmentation, random initialisation is used. We tune the parameter p which varies from 0 to 1 in FLILp to get the optimal result. In the following, we will show that the optimal p -value depends on the noise and the image. Generally, $p = 1$ is good for GN corrupted image, and smaller p is good for SPN corrupted image.

To display the segmentation result, we assign the grey level or colour value of the centre to each class. Note that for the visual comparison of methods on the synthetic images, we only display the results obtained by six methods including FCM, EnFCM, FLICM, FLILp, the better one between FCM_S1 and FCM_S2, and the best one among FGFCM, FGFCM_S1 and FGFCM_S2.

For fair comparison, all the experiments are performed under Windows 8 and MATLAB R2012a with Intel Core i7-4500 CPU@1.80 GHz and 8GB memory.

4.1 Test on two-phase synthetic image

In the first test, we perform the nine algorithms on a two-phase synthetic image which is contaminated by different levels of GN and SPN. The mean of GN is zero and the standard deviation varies from 10 to 60. The levels of SPN vary from 10 to 60%. The comparison of SA of different methods is reported in Table 1. The test images and experimental results are partially displayed in Figs. 2–4. The best SA values are marked in bold. We provide a

detailed analysis of Table 1, Figs. 3 and 4 in the following sections.

From Table 1, for GN, we observe that as the noise-level increases, the SA value of FCM decreases much faster than others. It shows that FCM is very sensitive to higher-level GN. By incorporating some smoothing terms, the other methods are much more robust to noise than FCM. The median filter-based variants FCM_S2 and FGFCM_S2 have slightly lower SA values than other variants of FCM. Among all, the proposed FLILp algorithm gets the highest SA values. FLICM is the second best, which achieves the same performance as FLILp when $\sigma \leq 40$. For SPN, the SA values of FCM are quite low compared with others, which shows that FCM is very sensitive to this kind of noise. Since the mean filter is not good for SPN, S1-type methods works not so good as other variants of FCM. S2-type variants FCM_S2 and FGFCM_S2 work well in this test and have similar performance. Among all, the proposed FLILp method gives the most accurate segmentation and achieves the highest SA values 1 for all the six noise levels. Note that we set $p = 1$ for GN and $p = 0.01$ for SPN to get the optimal results.

In Fig. 2, we show the clean synthetic image and its noisy versions. In Fig. 3, we display the results of the six methods applied to the Gaussian noisy image with standard deviation 60 in Fig. 2b. It is obvious that the FCM result in Fig. 3a is very noisy since a large amount of pixels are misclassified. Although better than the result of FCM, there are still many spots in the results of FCM_S1, EnFCM, FGFCM_S1 as displayed in Figs. 3b–d. The result of FLICM in Fig. 3e and the result of FLILp in Fig. 2f are much cleaner than others where the errors only occur on the middle

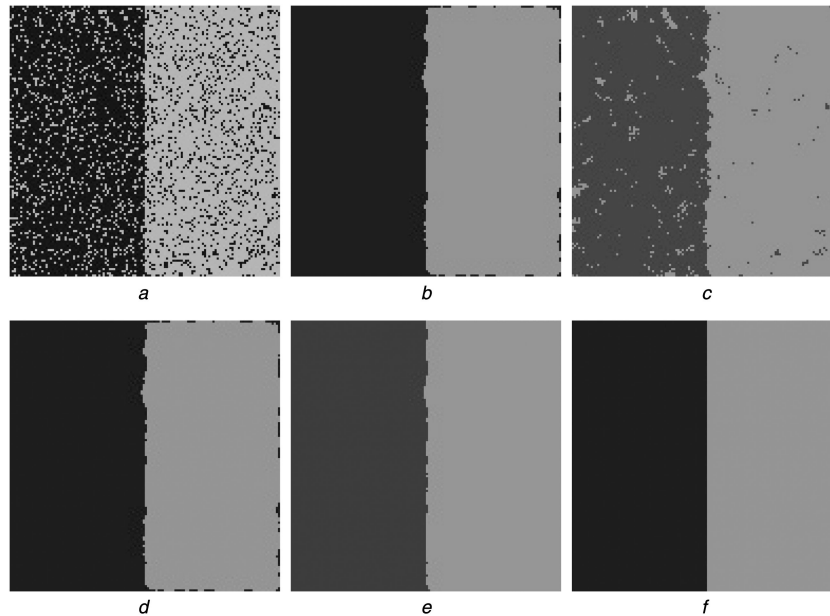


Fig. 4 Four-phase segmentation of a synthetic image corrupted by SPN

(a) FCM result, 0.8478; (b) FCM_S2 result, 0.9895; (c) EnFCM result, 0.9670; (d) FGFCM_S2 result, 0.9895; (e) FLICM result, 0.9968; (f) FLILp result, 1. The SA values are reported below each segmentation result

Table 1 SA of different methods for the synthetic image polluted by GN and SPN with different level in Fig. 1a

| | 10 | 20 | 30 | 40 | 50 | 60 |
|----------------------|--------|--------|--------|---------------|---------------|---------------|
| GN (σ) | | | | | | |
| FCM | 1 | 0.9970 | 0.9642 | 0.9146 | 0.8627 | 0.8161 |
| FCM_S1 | 1 | 1 | 0.9998 | 0.9988 | 0.9978 | 0.9919 |
| FCM_S2 | 0.9998 | 0.9993 | 0.9991 | 0.9978 | 0.9939 | 0.9794 |
| EnFCM | 1 | 1 | 0.9997 | 0.9988 | 0.9978 | 0.9915 |
| FGFCM | 1 | 1 | 0.9998 | 0.9994 | 0.9984 | 0.9899 |
| FGFCM_S1 | 1 | 0.9998 | 0.9988 | 0.9977 | 0.9967 | 0.9927 |
| FGFCM_S2 | 0.9998 | 0.9993 | 0.9988 | 0.9969 | 0.9921 | 0.9776 |
| FLICM | 1 | 1 | 1 | 0.9996 | 0.9988 | 0.9974 |
| FLILp ($p = 1$) | 1 | 1 | 1 | 0.9996 | 0.9990 | 0.9979 |
| SPN (%) | | | | | | |
| FCM | 0.9480 | 0.8983 | 0.8478 | 0.7979 | 0.7486 | 0.6980 |
| FCM_S1 | 0.9980 | 0.9868 | 0.9684 | 0.9252 | 0.8797 | 0.8094 |
| FCM_S2 | 0.9983 | 0.9949 | 0.9895 | 0.9850 | 0.9742 | 0.9561 |
| EnFCM | 0.9977 | 0.9882 | 0.9670 | 0.9268 | 0.8790 | 0.8135 |
| FGFCM | 0.9987 | 0.9898 | 0.9740 | 0.9316 | 0.8846 | 0.8120 |
| FGFCM_S1 | 0.9978 | 0.9913 | 0.9781 | 0.9503 | 0.8920 | 0.8309 |
| FGFCM_S2 | 0.9983 | 0.9949 | 0.9895 | 0.9850 | 0.9742 | 0.9561 |
| FLICM | 0.9995 | 0.9987 | 0.9968 | 0.9954 | 0.9922 | 0.9857 |
| FLILp ($p = 0.01$) | 1 | 1 | 1 | 1 | 1 | 1 |

edge. Moreover, the edge is better preserved by FLICM and FLILp than others. In Fig. 4, we display the results of the six methods applied to the image with 30% SPN. The result of FCM in Fig. 4a is quite noisy since a large amount of pixels are misclassified. There are many spots in the results of EnFCM in Fig. 4c. The results of FCM_S2, FGFCM_S2 and FLICM are cleaner than FCM and EnFCM. Among these three methods, the result of FLICM seems better than the other two. Among all, the proposed FLILp gives the most accurate and satisfactory results. Moreover, the middle edge is accurately preserved by FLILp. In terms of SA, FLILp achieves the best performance.

4.2 Test on four-phase synthetic image

In this test, we apply the nine methods to a four-phase synthetic image which is also contaminated by GN with mean zero and standard deviation ranging from 10 to 60, and SPN ranging from 10 to 60%, respectively. The SA of different methods is reported in

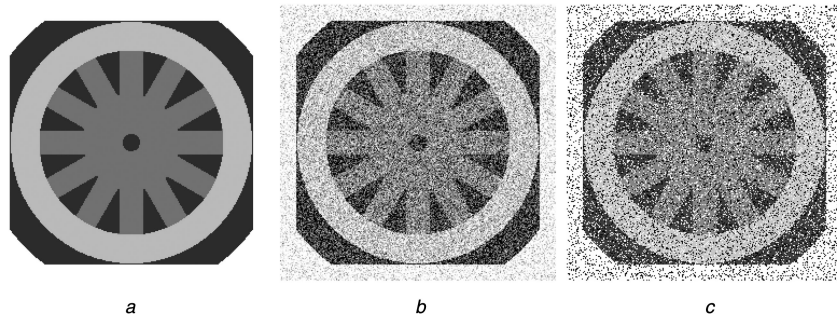
Table 2. The test images and experimental results are partially displayed in Figs. 5–7. Note that we set $p = 0.3$ for SPN with noise level not >30 and $p = 1$ for the others.

From Table 2, we find that the SA values of FCM decrease rapidly as the noise-level increase. All the variants of FCM perform better than FCM when $\sigma \geq 20$. For GN with $\sigma \geq 30$, both FLICM and FLILp achieve much higher SA value than others. Meanwhile, FLILp achieves the best performance among all.

In Fig. 5, we display the clean four-phase synthetic test image and its noisy version. Fig. 6 shows that for GN with $\sigma = 60$, the segmentation results of FLICM and FLILp are much cleaner than others. For SPN, S2-type methods perform much better than S1-type methods. We also find that FLICM performs poorly for noise-level $>30\%$. Among all, the proposed FLILp algorithm achieves the best SA value. Fig. 7 shows that for 30% SPN, the results of FCM_S2, FGFCM_S2, FLICM and FLILp are much cleaner than others. It is obvious that FLILp gives the best segmentation result

Table 2 SA of different methods for the synthetic image polluted by GN and SPN with different level in Fig. 4a

| | 10 | 20 | 30 | 40 | 50 | 60 |
|------------------------|---------------|---------------|---------------|---------------|---------------|---------------|
| GN (σ) | | | | | | |
| FCM | 0.9997 | 0.9415 | 0.8186 | 0.7130 | 0.6316 | 0.5701 |
| FCM_S1 | 0.9569 | 0.9561 | 0.9536 | 0.9449 | 0.9220 | 0.8894 |
| FCM_S2 | 0.9981 | 0.9954 | 0.9818 | 0.9521 | 0.9080 | 0.8575 |
| EnFCM | 0.9569 | 0.9560 | 0.9536 | 0.9433 | 0.9162 | 0.8749 |
| FGFCM | 0.9704 | 0.9702 | 0.9661 | 0.9501 | 0.9167 | 0.8688 |
| FGFCM_S1 | 0.9549 | 0.9523 | 0.9499 | 0.9406 | 0.9162 | 0.8794 |
| FGFCM_S2 | 0.9980 | 0.9945 | 0.9799 | 0.9427 | 0.8911 | 0.8214 |
| FLICM | 0.9954 | 0.9906 | 0.9824 | 0.9741 | 0.9662 | 0.9531 |
| FLILp ($p = 1$) | 0.9999 | 0.9953 | 0.9875 | 0.9782 | 0.9707 | 0.9587 |
| SPN (%) | | | | | | |
| FCM | 0.9236 | 0.8480 | 0.7717 | 0.6971 | 0.6244 | 0.5487 |
| FCM_S1 | 0.8867 | 0.8052 | 0.7604 | 0.7428 | 0.6484 | 0.5684 |
| FCM_S2 | 0.9931 | 0.9855 | 0.9724 | 0.9639 | 0.9508 | 0.9224 |
| EnFCM | 0.9102 | 0.8030 | 0.6953 | 0.7465 | 0.6407 | 0.5583 |
| FGFCM | 0.9528 | 0.9061 | 0.8342 | 0.8157 | 0.7248 | 0.6152 |
| FGFCM_S1 | 0.8996 | 0.7890 | 0.7084 | 0.7586 | 0.6700 | 0.5670 |
| FGFCM_S2 | 0.9907 | 0.9873 | 0.9755 | 0.9748 | 0.9649 | 0.9389 |
| FLICM | 0.9936 | 0.9857 | 0.9649 | 0.7333 | 0.4834 | 0.4794 |
| FLILp ($p = 0.3, 1$) | 0.9979 | 0.9953 | 0.9914 | 0.9763 | 0.9718 | 0.9607 |

**Fig. 5** Four-phase synthetic image and noisy images

(a) The clean synthetic image with grey-level values 43, 112, 185 and 255, (b) The noisy image corrupted by GN with mean zero and standard deviation $\sigma = 60$, (c) The noisy image corrupted by 30% SPN

among all. Furthermore, it is obvious that the edges are better preserved by FLILp than others in the segmentation results.

4.3 Test on real colour images

Finally, we test the proposed algorithm FLILp on real colour images in Figs. 8 and 9 for two-phase and multiphase ($c > 2$) segmentation, respectively. Since there is no ground truth of segmentation, we can only compare the results visually. In Figs. 8 and 9, the left column shows the real images, the second column shows the results of FCM algorithm and the right column displays the image segmentation results of the proposed FLILp algorithm. The results of our method are more satisfactory than FCM. The results of FCM contain many tiny components which belong to incorrect clusters. While in the results of our FLILp, the tiny components are successfully smoothed out by incorporating local information and using L_p norm distance. Moreover, the sharp edges between different clusters in the images are preserved well by FLILp.

4.4 Computational complexity and time

As discussed in [24], the computational complexity of FCM is $O(nc)$ where n is the length of the histogram and c is the number of classes. Hence, the FCM variations including EnFCM, FGFCM, FGFCM_S1 and FGFCM_S2 have the same complexity with some variation depending on the preprocessing steps in each algorithm. The computational complexity of FCM_S1, FCM_S2, FLICM and the proposed FLILp is $O(Nc)$ where N is the total number of pixels.

In terms of computational time, the proposed FLILp method is more time-consuming than others. For example, for the first test image with size 128×128 , the average computational time corresponding to Table 1 is about 0.0430 s for FCM, 0.0364 s for FCM_S1, 0.0339 s for FCM_S2, 0.0208 s for EnFCM, 0.1628 s for FGFCM, 0.0208 s for FGFCM_S1, 0.0247 s for FGFCM_S2, 0.1823 s for FLICM, and 0.6289 s for FLILp, where 's' denotes seconds. However, this disadvantage of the proposed FLILp method is compensated for its outstanding performance as shown above. Moreover, the proposed algorithm can be speeded up by including parallel computing techniques which is our future work.

5 Conclusion

In this paper, a novel fuzzy local information and L_p -norm distance (FLILp)-based clustering method was proposed for image segmentation. Both of the local spatial information and colour information are incorporated into the objective function by a novel fuzzy factor. In both the global and local penalty terms, L_p -norm is used to measure the distance of image data to its cluster centres, which is different from all the existing variants of FCM. The numerical difficulty caused by L_p -norm is overcome by regarding it as weighted L_2 -norm. Benefited from both the local factor and the L_p -norm distance, the proposed FLILp outperforms the existing variants of FCM in terms of noise immunity and SA.

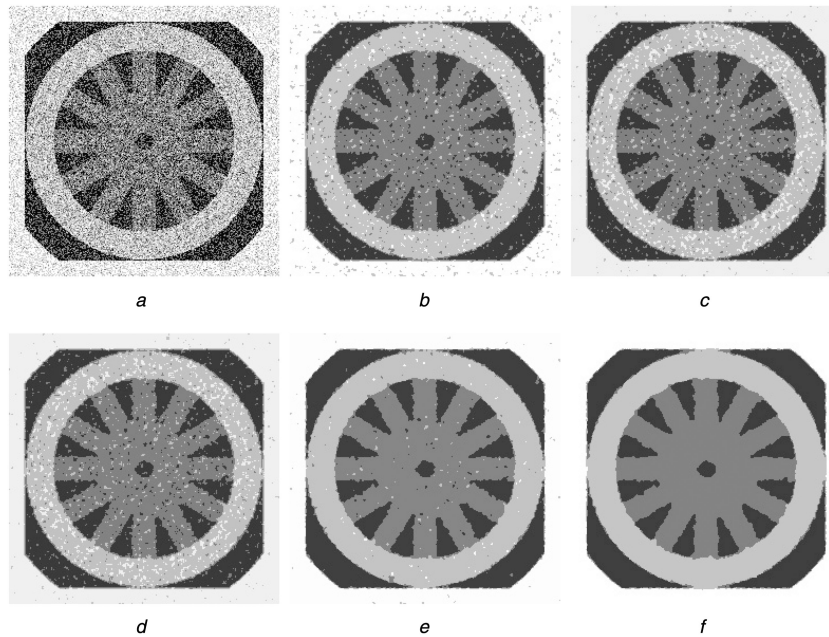


Fig. 6 Four-phase segmentation of a synthetic image corrupted by GN
 (a) FCM result, 0.5701; (b) FCM_S1 result, 0.8894; (c) EnFCM result, 0.8749; (d) FGFCM_S1 result, 0.8794; (e) FLICM result, 0.9531 (f) FLILp result, 0.9587. The SA values are reported below each segmentation result

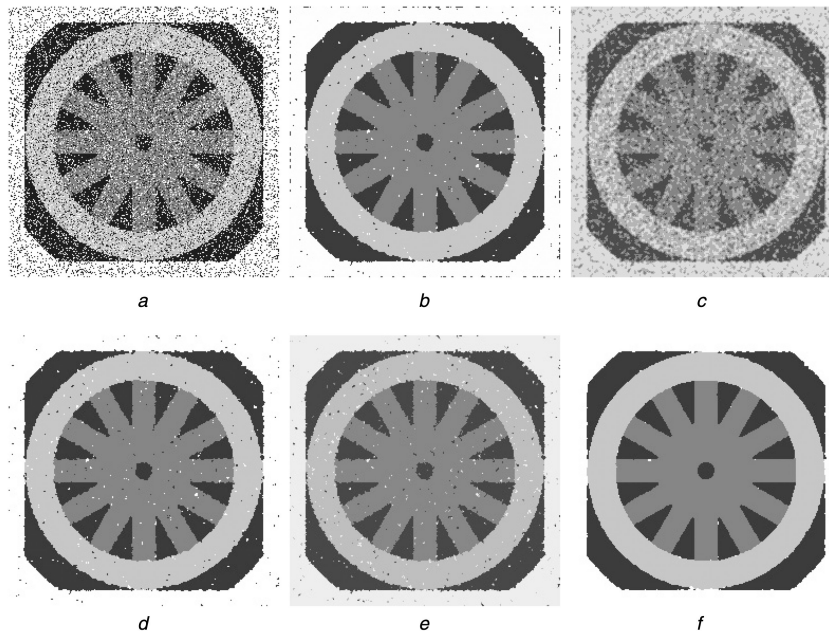


Fig. 7 Two-phase segmentation of a synthetic image corrupted by SPN
 (a) FCM result, 0.7717; (b) FCM_S2 result, 0.9724; (c) EnFCM result, 0.6953; (d) FGFCM_S2 result, 0.9755; (e) FLICM result, 0.9649; (f) FLILp result, 0.9914. The SA values are reported below each segmentation result

6 Acknowledgments

The research of F. Li is supported by the National Science Foundation of China (No. 11671002) and the Science and Technology Commission of Shanghai Municipality (STCSM) (No. 13dz2260400). The research of Jing Qin is supported by the faculty start-up fund of Montana State University.

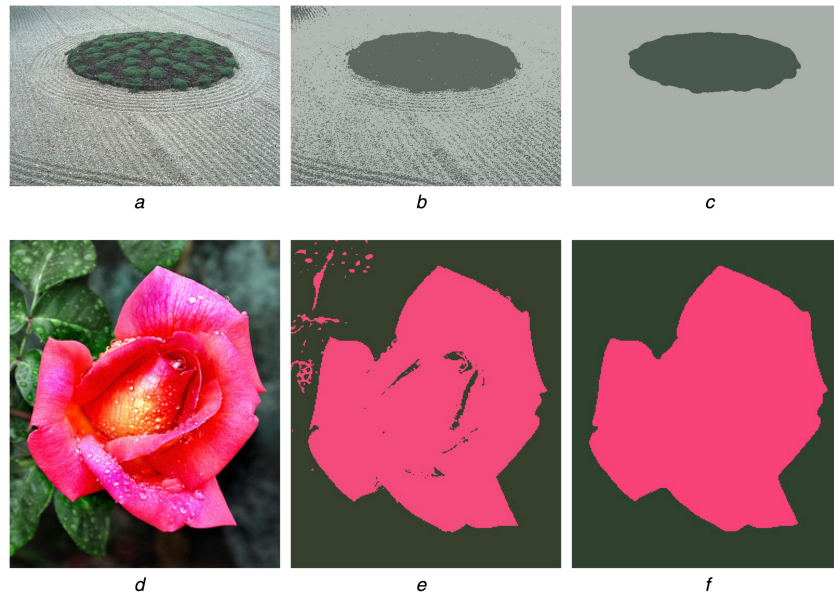


Fig. 8 Two-phase segmentation results on real colour images

(a, d): Original images; (b, e): The segmentation results by FCM, $c=2$; (c, f): The segmentation results by the proposed algorithm FLILp, $c=2$

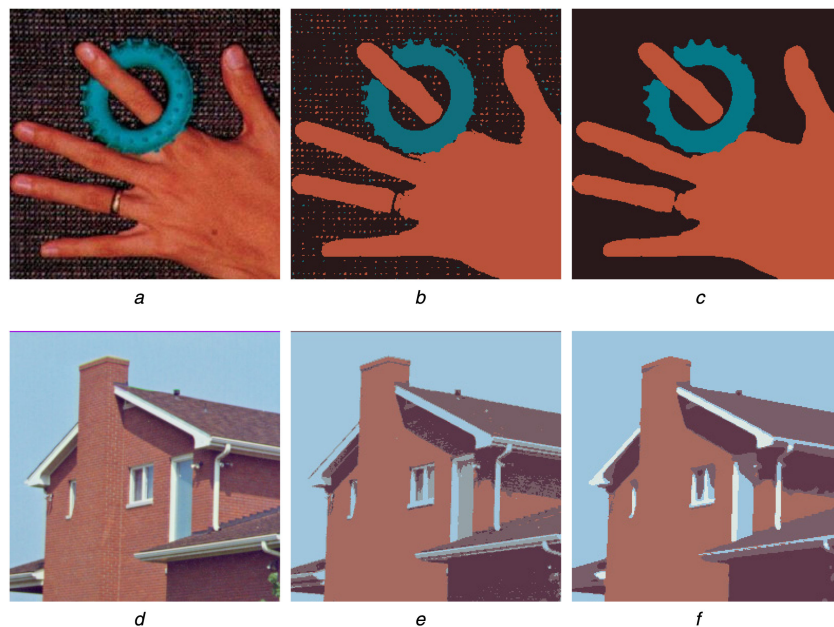


Fig. 9 Multiphase segmentation results on real colour images

(a, d): Original images; (b, e): The segmentation results by FCM; (c, f): The segmentation results by the proposed algorithm FLILp. The cluster numbers are 3 and 5 for the first and the second rows, respectively

7 References

- [1] Balafar, M.A., Ramli, A.R., Iqbal Saripan, M., *et al.*: 'Review of brain MRI image segmentation methods', *Artif. Intell. Rev.*, 2010, **33**, (3), pp. 261–274
- [2] Cheng, M.-M., Mitra, N.J., Huang, X., *et al.*: 'Global contrast based salient region detection', *IEEE Trans. Pattern Anal. Mach. Intell.*, 2015, **37**, (3), pp. 569–582
- [3] Ilea, D.E., Whelan, P.F.: 'Image segmentation based on the integration of colour–texture descriptors: a review', *Pattern Recogn.*, 2011, **44**, (10), pp. 2479–2501
- [4] Lucchesevz, L., Mitray, S.K.: 'Color image segmentation: A state-of-the-art survey', *Proc. Indian Natl. Sci. Acad. (INSA-A)*, 2001, **67**, (2), pp. 207–221
- [5] Muñoz, X., Freixenet, J., Cufí, X., *et al.*: 'Strategies for image segmentation combining region and boundary information', *Pattern Recognit. Lett.*, 2003, **24**, (1), pp. 375–392
- [6] Wang, Q., Yuan, Y., Yan, P.: 'Visual saliency by selective contrast', *IEEE Trans. Circuits Syst. Video Technol.*, 2013, **23**, (7), pp. 1150–1155
- [7] Wang, Q., Yuan, Y., Yan, P., *et al.*: 'Saliency detection by multiple-instance learning', *IEEE Trans. Cyber.*, 2013, **43**, (2), pp. 660–672
- [8] Yuan, Y., Lin, J., Wang, Q.: 'Dual-clustering-based hyperspectral band selection by contextual analysis', *IEEE Trans. Geosci. Remote Sens.*, 2016, **54**, (3), pp. 1431–1445
- [9] Zhu, S.C., Yuille, A.: 'Region competition: Unifying snakes, region growing, and bayes/mdl for multiband image segmentation', *IEEE Trans. Pattern Anal. Mach. Intell.*, 1996, **18**, (9), pp. 884–900
- [10] Bezdek, J.C., Ehrlich, R., Full, W.: 'Fcm: The fuzzy c-means clustering algorithm', *Comput. Geosci.*, 1984, **10**, (2), pp. 191–203
- [11] Dunn, J.C.: 'A fuzzy relative of the isodata process and its use in detecting compact well-separated clusters', *Cybern. Syst.*, 1973, **3**, (3), pp. 32–57
- [12] Leski, J.: 'Towards a robust fuzzy clustering', *Fuzzy Sets Syst.*, 2003, **137**, (2), pp. 215–233
- [13] Noordam, J.C., Van den Broek, W.H.A.M., Buydens, L.M.C.: 'Geometrically guided fuzzy c-means clustering for multivariate image segmentation'. Proc. 15th Int. Conf. on Pattern Recognition, 2000., 2000, vol. **1**, pp. 462–465
- [14] Pal, N.R., Pal, K., Keller, J.M., *et al.*: 'A possibilistic fuzzy c-means clustering algorithm', *IEEE Trans. Fuzzy Syst.*, 2005, **13**, (4), pp. 517–530
- [15] Xu, R., Wunsch, D.: 'Survey of clustering algorithms', *IEEE Trans. Neural Netw.*, 2005, **16**, (3), pp. 645–678
- [16] Bezdek, J.C., Hathaway, R.J., Sabin, M.J., *et al.*: 'Convergence theory for fuzzy c-means: counterexamples and repairs', *IEEE Trans. Syst. Man Cybern.*, 1987, **17**, (5), pp. 873–877
- [17] Pham, D.L.: 'Spatial models for fuzzy clustering', *Comput. Vis. Image Underst.*, 2001, **84**, (2), pp. 285–297
- [18] Ahmed, M.N., Yamany, S.M., Mohamed, N., *et al.*: 'A modified fuzzy c-means algorithm for bias field estimation and segmentation of mri data', *IEEE Trans. Med. Imaging*, 2002, **21**, (3), pp. 193–199

- [19] Bae, E., Tai, X.-C.: 'Efficient global minimization methods for image segmentation models with four regions', *J. Math. Imaging Vis.*, 2015, **51**, (1), pp. 71–97
- [20] Cai, W., Chen, S., Zhang, D.: 'Fast and robust fuzzy c-means clustering algorithms incorporating local information for image segmentation', *Pattern Recogn.*, 2007, **40**, (3), pp. 825–838
- [21] Chen, S., Zhang, D.: 'Robust image segmentation using FCM with spatial constraints based on new kernel-induced distance measure', *IEEE Trans. Syst. Man Cybern. B Cybern.*, 2004, **34**, (4), pp. 1907–1916
- [22] Chuang, K.-S., Tzeng, H.-L., Chen, S., *et al.*: 'Fuzzy c-means clustering with spatial information for image segmentation', *Comput. Med. Imaging Graph.*, 2006, **30**, (1), pp. 9–15
- [23] Kang, B.-Y., Kim, D.-W., Li, Q.: 'Spatial homogeneity-based fuzzy c-means algorithm for image segmentation'. *Fuzzy Systems and Knowledge Discovery*, 2005, pp. 462–469
- [24] Krinidis, S., Chatzis, V.: 'A robust fuzzy local information c-means clustering algorithm', *IEEE Trans. Image Process.*, 2010, **19**, (5), pp. 1328–1337
- [25] Li, C., Gatenby, C., Wang, L., *et al.*: 'A robust parametric method for bias field estimation and segmentation of MR images'. *IEEE Conf. on Computer Vision and Pattern Recognition*, 2009 (CVPR 2009), 2009, pp. 218–223
- [26] Li, F., Shen, C., Li, C.: 'Multiphase soft segmentation with total variation and H1 regularization', *J. Math. Imaging Vis.*, 2010, **37**, (2), pp. 98–111
- [27] Li, Z., Zeng, T.: 'A two-stage image segmentation model for multi-channel images', *Commun. Comput. Phys.*, 2016, **19**, (4), pp. 904–926
- [28] Pham, D.L.: 'Fuzzy clustering with spatial constraints'. *Proc. 2002 Int. Conf. on Image Processing*. 2002., 2002, vol. **2**, pp. 65–68
- [29] Sikka, K., Sinha, N., Singh, P.K., *et al.*: 'A fully automated algorithm under modified FCM framework for improved brain MR image segmentation', *Magn. Reson. Imaging*, 2009, **27**, (7), pp. 994–1004
- [30] Szilagy, L., Benyo, Z., Szilagy, S.M., *et al.*: 'Mr Brain image segmentation using an enhanced fuzzy c-means algorithm'. *Engineering in Medicine and Biology Society*, 2003. *Proc. of the 25th Annual Int. Conf. of the IEEE*, 2003, vol. **1**, pp. 724–726
- [31] Wang, J., Kong, J., Lu, Y., *et al.*: 'A modified FCM algorithm for mri brain image segmentation using both local and non-local spatial constraints', *Comput. Med. Imaging Graph.*, 2008, **32**, (8), pp. 685–698
- [32] Hathaway, R.J., Bezdek, J.C., Hu, Y.: 'Generalized fuzzy c-means clustering strategies using l p norm distances', *IEEE Trans. Fuzzy Syst.*, 2000, **8**, (5), pp. 576–582
- [33] Jajuga, K.: 'L1-norm based fuzzy clustering', *Fuzzy Sets Syst.*, 1991, **39**, (1), pp. 43–50
- [34] Kersten, P.R.: 'Implementation issues in the fuzzy c-medians clustering algorithm'. *Proc. of the Sixth IEEE Int. Conf. on Fuzzy Systems*, 1997., 1997, vol. **2**, pp. 957–962
- [35] Kersten, P.R.: 'The fuzzy median and the fuzzy MAD'. *Proc. of ISUMA-NAFIPS'95, Third Int. Symp. on Uncertainty Modeling and Analysis*, 1995, and *Annual Conf. of the North American Fuzzy Information Processing Society*, 1995, pp. 85–88
- [36] Guo, X., Li, F., Ng, M.K.: 'A fast l1-TV algorithm for image restoration', *SIAM J. Sci. Comput.*, 2009, **31**, (3), pp. 2322–2341
- [37] Nikolova, M.: 'A variational approach to remove outliers and impulse noise', *J. Math. Imaging Vis.*, 2004, **20**, (1–2), pp. 99–120